ChemElectroChem | doi.org/10.1002/celc.202001488

European Chemical Societies Publishing

Special Collection

Influence of Complexing Additives on the Reversible Deposition/Dissolution of Magnesium in an Ionic Liquid

Isabella Weber,[a, b, c] Johannes Ingenmey,[d] Johannes Schnaidt,[a, b, c] Barbara Kirchner,[d] and R. Jürgen Behm*[a, b]

Aiming at a fundamental understanding of the synergistic effects of different additives on the electrochemical Mg deposition/dissolution in an ionic liquid, we have systematically investigated these processes in a combined electrochemical and theoretical study, using 1-butyl-1-methylpyrrolidinium bis (trifluoromethylsulfonyl) imide (BMP-TFSI) as the solvent and a cyclic ether (18-crown-6) and magnesium borohydride as additives. Both crown ether and BH_4^- improve Mg deposition, its reversibility, and cycling stability. The combined presence of both additives and their concentration relative to that of Mg^{2+} are decisive for more facile and reversible Mg deposition/dissolution. These results and those of quantum chemical calculations indicate that 18-crown-6 can partly displace $TFSI^-$ from its direct coordination to Mg^{2+}. Furthermore, the interaction between Mg^{2+} and directly coordinated $TFSI^-$ is weakened by coordination with 18-crown-6, preventing its Mg^+-induced decomposition. Finally, Mg deposition is improved by the weaker overall coordination upon Mg^{2+} reduction to Mg^+.

1. Introduction

Despite of the advantages of rechargeable Mg batteries in comparison to conventional lithium-ion batteries (LIBs), such as their generally higher energy density, the possibility of using elemental Mg anodes, the global availability and non-toxicity of Mg, and their recyclability and low costs,[1–8] their technical verification and commercial introduction is still far away. This is mainly due to problems in the reversible deposition and dissolution of Mg, which are – at least in part – related to complications arising from reductive electrolyte decomposition at the anode|electrolyte interface. In contrast to LIBs, where Li^+ transport is possible through the so-called solid electrolyte interphase (SEI) formed at the anode during charge/discharge, these layers often inhibit the Mg deposition/dissolution process.[2,3,9] Only recently, studies reported on a functional SEI formed upon Mg deposition, e.g., from $Mg(BH_4)_2$/$LiBH_4$-containing monoglyme,[10] in Mg/S systems,[11] or on Sn-modified anodes.[12] In general, most investigations so far have focused on salt/solvent combinations that allow reversible Mg deposition/dissolution without the formation of a protective surface layer. Among those, a limited number of electrolytes consisting of commercially available magnesium salts such as $Mg(BH_4)_2$[13–20] or $Mg((CF_3SO_2)_2N)_2$ (Mg bis (trifluoromethylsulfonyl)imide, $MgTFSI_2$)[20–27] have been found to support largely reversible Mg plating and stripping without negative impact on the cell components (such as corrosion, which poses a problem in Cl-containing electrolytes).[4] However, even for these electrolytes, the oxidative instability of the borohydride,[6] as well as the Mg^{2+}-[18,28] and moisture-induced[16,25,29,30] decomposition of $TFSI^-$, severely limit their application. Hence, the development of suitable electrolytes allowing for reversible Mg plating/stripping is still of utmost importance for the introduction of rechargeable Mg-based batteries.[3,31–36]

Ionic liquids (ILs) are a promising alternative to electrolytes based on organic solvents due to their generally low flammability, high electrochemical stability, and low vapor pressure.[16,37,38] Specifically, $TFSI^-$-based ILs have attracted interest due to their relatively high conductivity, their commercial availability, and the simplicity of the system when adding $MgTFSI_2$ as Mg salt. This approach, however, has turned out to be little successful so far, as the reductive decomposition of $TFSI^-$, which is promoted by the interaction with the Mg^{2+} species,[39–42] leads to the formation of passivating films (in particular on Mg metal electrodes[32]). The successful use of IL-based electrolytes thus requires either ionic liquids that are stable in the entire potential range also upon interaction with Mg^{2+}, or the development of additives that could lower any

[a] I. Weber, Dr. J. Schnaidt, Prof. Dr. R. J. Behm
Institute of Surface Chemistry and Catalysis
Ulm University
Albert-Einstein-Allee 47, 89081 Ulm, Germany
E-mail: juergen.behm@uni-ulm.de
[b] I. Weber, Dr. J. Schnaidt, Prof. Dr. R. J. Behm
Helmholtz Institute Ulm (HIU) Electrochemical Energy Storage
Helmholtzstraße 11, 89081 Ulm, Germany
[c] I. Weber, Dr. J. Schnaidt
Karlsruhe Institute of Technology (KIT)
P.O. Box 3640
76021 Karlsruhe, Germany
[d] J. Ingenmey, Prof. Dr. B. Kirchner
Mulliken Center for Theoretical Chemistry
Bonn University
Beringstraße 4, 53114 Bonn, Germany

Supporting information for this article is available on the WWW under https://doi.org/10.1002/celc.202001488

An invited contribution to a joint Special Collection between ChemElectroChem and Batteries & Supercaps dedicated to research Beyond Lithium-Ion Batteries

detrimental interaction between Mg^{2+} and the IL – while still allowing reversible Mg deposition/dissolution.

This is the topic of the present paper, where we report results of a combined experimental and theoretical study on the effect of two different additives, the crown ether 18-crown-6 and borohydride (BH_4^-), on the deposition/dissolution of Mg from the IL 1-butyl-1-methylpyrrolidinium bis (trifluoromethylsulfonyl)imide (BMP-TFSI) using $MgTFSI_2$ and, where present, $Mg(BH_4)_2$ as Mg^{2+} source. Glassy carbon (GC) and, for comparison with realistic battery systems, Mg, were used as working electrodes. In this work, we are especially interested in a basic mechanistic understanding of the interplay between Mg^{2+}, the anion $TFSI^-$ and the additives $Mg(BH_4)_2$ and 18-crown-6, and particularly in synergistic effects. A semi-quantitative understanding shall be derived by systematically varying the composition of the electrolyte, both in experiment and in simulations. Here, it is important that stabilization of the electrolyte does not inhibit Mg deposition. Furthermore, the role of the electrode shall be elucidated by comparing results obtained for the rather inert GC model electrodes and the more reactive, realistic Mg electrodes.

While there is a considerable number of studies investigating the Mg–TFSI interaction in organic solvents such as DME, THF or polyethers/glymes,[18,19,28,30,43–48] the number of studies performed in electrolytes using a $TFSI^-$-containing IL as main component is much less, and such kind of insights as aimed at in the present study have not been reported so far.[16,17,39–41] Finally, the idea of adding a complexing additive was followed also in a study by Watkins *et al.*, who prepared chelating ILs by adding a polyether chain to the cation.[17] Compared to that approach, ours seems to be experimentally simpler and more feasible. On the other hand, combining chelating solvents such as glymes with an IL-based Mg source such as $MgTFSI_2$ (see above) may lose the advantages of a mainly IL-based electrolyte.

The crown ether is a typical complexing agent[49] and has previously been employed to, e.g., enhance Mg plating/stripping in an ionic liquid.[40,42] $Mg(BH_4)_2$ has been repeatedly used as water scavenger in IL-containing electrolytes.[16,17,19,30,43,44,50] It was reported to prevent the formation of a passivating surface layer in $TFSI^-$-based electrolytes[51] and also serves as Mg source.[14] Furthermore, BH_4^- has been proposed to act as Mg^{2+}-complexing agent[15,16] and/or interact with the anode surface; either by adsorption (similar to chloride-containing electrolytes[52]) or by dissolving passivation layers either during formation or pre-existing ones (native passivation layers) due to its highly reductive character.

In the following, we will first present cyclic voltammetry data on the Mg deposition/dissolution behavior on glassy carbon from a BMP-TFSI-based electrolyte containing either $Mg(BH_4)_2$ or a combination of $Mg(BH_4)_2$ and crown ether. Next, we show results of similar experiments using electrolytes containing also $MgTFSI_2$, where, for a better understanding of possible synergistic effects, the concentrations of the different components were varied systematically. For comparison, we also show data obtained for Mg deposition/dissolution from similar electrolytes on a Mg electrode. Subsequently, we present results of a DFT-based quantum chemical analysis of the stability of clusters derived from classical molecular dynamics (MD) simulations, which contain Mg^{2+} in different coordination states and up to two BMP-TFSI ion pairs with or without 18-crown-6 as additional ligand. Finally, we discuss the implications of both the experimental and theoretical data and summarize the main conclusions derived from these data.

2. Results and Discussion

2.1. Electrochemical Characterization

In previous experiments, we had already shown that deposition and dissolution of Mg on a glassy carbon (GC) electrode is essentially inhibited in $MgTFSI_2$-containing BMP-TFSI electrolyte.[41] This was reproduced also in the present experiments, though some improvement is achieved for $Mg(BH_4)_2$-containing BMP-TFSI electrolytes. The first and later cycles of the CVs recorded at 10 $mV\,s^{-1}$ on the GC substrate, without any additional additives, largely resemble previous findings.[17] They are displayed and discussed in detail with Figure S1a and b. In brief, the negative current increases towards the lower potential limit. A small anodic peak appears at around 1 V in the anodic scan. Within the first few cycles, both peaks decrease significantly. The overall reversibility of the cathodic and anodic processes, as indicated by the overall charge ratio in these potential regimes (Coulombic efficiency), is about 18% in the first cycle (inset in Figure S1a) and increases to around 35% in subsequent cycles (see Figure S4 and Table S1). Overall, however, the reversibility is very low and Mg deposition/dissolution is (at most) a minor process.

In the following, we will briefly summarize the different effects and influences of borohydride on the Mg deposition/dissolution process that have been reported in the past. First, the addition of reductive, contamination-scavenging additives such as di-butyl Mg (in our case: $Mg(BH_4)_2$), which can react with traces of water, oxygen and other protic species, was found to improve the Mg plating/stripping efficiency by forming Mg oxides and hydroxides in the bulk, which, in return, reduces/avoids surface passivation.[30,51] Second, reversible Mg plating/stripping was found to require a minimum amount of such additives, which approximately corresponded to a slight excess relative to the estimated water content of the electrolyte.[30] Third, reversible Mg plating/stripping was possible also from $MgTFSI_2$-containing solutions when using complexing solvents such as glymes upon addition of $Mg(BH_4)_2$[30] or once the electrolyte was carefully dried.[25] Finally, high deposition reversibilities were obtained even without additional drying when using $Mg(BH_4)_2$ as Mg source rather than $MgTFSI_2$.[14]

Overall, these studies support the idea that borohydride acts as efficient water scavenger.[14,30] As stated above, our results of a very low reversibility for Mg plating/stripping fully agree with previous findings for cycling a Pt electrode in a similar electrolyte.[17,18] They seem to disagree, however, with the previous findings summarized above, considering that, in

our experiments, the amount of $Mg(BH_4)_2$ added to the electrolytes should always be sufficient to fully remove the water impurities of BMP-TFSI, $MgTFSI_2$ and crown ether, based both on our estimations and on the suppliers' specifications (see Experimental part) and assuming that each BH_4^- can react with one water molecule. The discrepancy is most likely caused by the different solvents, with only small amounts of $TFSI^-$ in the above cases, together with complexing solvents, while in our case the $TFSI^-$ is part of the solvent and thus present in large excess and no other complexing species are present.

Electrolyte decomposition in $Mg(BH_4)_2$-containing BMP-TFSI was explained by the decomposition of $TFSI^-$, which is coordinated with the metal ions in such IL mixtures. This kind of complex formation, where $TFSI^-$ anions can coordinate to a single metal cation (contact ion pairs, CIPs) or to multiple metal cations in aggregate networks (where the Mg^{2+} cation is in direct contact with the $TFSI^-$ anion), has been identified previously by both Infrared[16] and Raman spectroscopy.[17,18,53,54] Theoretical studies have shown that partial reduction of the Mg center, which is expected to happen at the interface at potentials in the Mg deposition regime, leads to a weakening of the C–S bond in the $TFSI^-$ anion, which in turn results in $TFSI^-$ decomposition rather than in Mg deposition.[18,28] In contrast, BH_4^- was found to be stable under these conditions. In electrolytes containing both borohydride and $TFSI^-$, $TFSI^-$ decomposition has been observed in experimental studies.[17,18,43,45,51,55]

Next, we investigated the influence of 18-crown-6 upon cycling in $Mg(BH_4)_2$-containing BMP-TFSI. CVs recorded in BMP-TFSI + 0.1 M $Mg(BH_4)_2$ + 0.1 M 18-crown-6 electrolyte are depicted in Figure 1. The additive leads to increased currents, both in the cathodic and in the anodic scan, as compared to the borohydride-containing IL in the absence of the crown ether (Figure S1). The cathodic current densities are at least four times higher and the increase of the anodic currents is even more drastic. These changes may originate from reversible processes, such as Mg plating and stripping, although the present data do not provide definite proof for the latter assignment. A weak peak is observed at −0.4 V in the first cathodic scan, which does not appear anymore in the subsequent cycles. Interestingly, in a crown ether-free, borohydride-containing IL, a similar signal appeared at −0.3 V in the first cathodic cycle (Figure S1a). We tentatively assign these peaks to the reductive removal of a surface contamination on the GC substrate, considering that this peak was only observed on the GC electrode, independent of the electrolyte composition. At potentials below −0.7 V, the characteristic current increase for Mg deposition appears. Here, Mg plating takes place with a nucleation overpotential that is by 0.1 V lower than the one observed for 0.1 M $Mg(BH_4)_2$-containing IL without any crown ether additive (see discussion with Figure S1). In the subsequent anodic scan, we find the corresponding signal for Mg dissolution at 0.3 V, down-shifted by 0.4 V from the Mg dissolution peak observed in crown ether-free IL. This is followed by two additional peaks at 0.4 V and 0.7 V, which seem to indicate that, next to Mg stripping, oxidation of species formed in cathodic side processes can take place under these conditions.

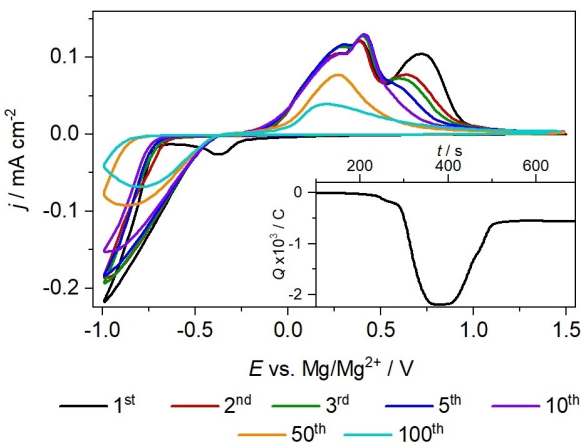

Figure 1. First and additional relevant potentiodynamic cycles recorded on a GC electrode in BMP-TFSI + 0.1 M $Mg(BH_4)_2$ + 0.1 M 18-crown-6 cycled at 10 mV s^{-1}. The inset shows the accumulated charge (i.e., the charge balance of Mg plating/stripping) during the first scan.

It is worth noting that the position of the peak at 0.7 V observed in the crown ether-containing system coincides with the position of the anodic peak recorded in the first cycles of the crown ether-free system (Figure S1). Therefore, it is also possible that the anodic signal at 0.7 V is due to Mg dissolution from a similar Mg species – as obtained for deposition from $Mg(BH_4)_2$-containing electrolyte – while the peaks at 0.3/0.4 V are due to dissolution of Mg deposits created in crown ether-containing electrolyte.

In the following cathodic scan, the process taking place at −0.4 V is inhibited, like the analogous process in the ether-free system. The decreasing currents in the Mg deposition region and, subsequently, in the Mg dissolution region (anodic scan), also indicate an increasing inhibition of the related processes and/or the depletion of oxidizable components with increasing cycling. This current loss is most pronounced for the high-potential peak at 0.7 V. During the next ten cycles, it decreases and disappears completely, while the anodic signals at 0.3 and 0.4 V do not change significantly. The peak at 0.4 V starts to decrease only after ten cycles and has disappeared after about 35 cycles (not shown). The signal at 0.3 V also decreases, but much slower, becoming the main anodic peak. It is still visible even after 100 cycles. The reversibility is about 70% in the first cycle (for comparison, the reversibility of the processes taking place in solely borohydride-containing IL was ~18% in the first cycle) and increases to 78% within the first ten cycles, as compared to 35% reached in ether-free electrolyte after the same number of cycles. Upon further cycling, however, the reversibility in the $Mg(BH_4)_2$- and 18-crown-6-containing IL decreases, as well, dropping to 25% after 20 cycles. This remains about constant for the rest of the cycling time (100 cycles in total), indicating that the continuing passivation process not only reduces the current densities both in the cathodic and anodic scan but also affects them in the same way, keeping the charge ratio between them constant (see Figure S5 and Table S2).

The results in Figure 1 can be compared with previous data and conclusions, which had already identified positive effects on the reversibility of the Mg plating/stripping process when modifying the IL cation[17–19] or varying the solvents and/or adding complexing additives.[15,19,42,56,57] Our results are in agreement with reports on an improved Mg deposition/dissolution reversibility in the presence of ethers such as glymes, etc.[21,30,47,58] As one example, Mandai *et al.* reported an improved Mg deposition/dissolution activity for tetraglyme-coordinated $MgTFSI_2$ in BMP-TFSI in the presence of dialkylsulfones as compared to electrolytes with less efficiently coordinating additives, such as DMSO.[47] Increased current densities for Mg deposition in $MgTFSI_2$-containing electrolytes were reported also by Sagane *et al.* upon addition of 18-crown-6 ether, both in THF[57] and in N-methyl-N-propylpiperidinium (MPPp)–TFSI.[42] Similarly, Ma *et al.* have shown reversible and stable (for more than 280 cycles) Mg plating and stripping from 0.3 M $MgTFSI_2$-containing BMP-TFSI/tetraglyme mixtures (1 : 2) after treatment with 0.019 M $Mg(BH_4)_2$.[19]

Employing *ex situ* scanning electron microscopy (SEM) characterization, Sagane *et al.* also observed the formation of Mg dendrites in the Mg deposits formed from 0.5 M crown ether- and 0.5 M $MgTFSI_2$-containing THF, which could hardly be dissolved subsequently.[57] Going to much higher concentrations of both ether additive and $TFSI^-$ salt in an IL electrolyte ($MgTFSI_2$, 18-crown-6 and MPPp–TFSI, with molar ratios of 1 : 1 : 5 and 1 : 5 : 5), the Mg deposits were significantly smoother than the dendritic morphologies obtained in THF-based electrolyte, but still exhibited a 'mossy' structure, which the authors attributed to the high viscosity of the ionic liquid as well as to accelerated $TFSI^-$ decomposition.[42] We assume that this is also the reason for the poor reversibility of about 3% obtained in that study. This deposition/dissolution behavior is very different from the uniform Mg deposits obtained in Grignard-based electrolytes, which also allowed reversible dissolution.[59]

Watkins *et al.* had proposed that the addition of a chelating agent (in their case, oligoether glymes or 18-crown-6) separates the direct coordination of Mg^{2+} by $TFSI^-$ and results in the formation of $[(Mg(glyme)_x)^{2+}(TFSI^-)]^+$ complexes, which they referred to as solvent-separated ion pairs (SSIPs).[54] This was concluded from the disappearance of the Raman band typical for Mg^{2+}-coordinated $TFSI^-$ and the appearance of a new band that was associated with Mg^{2+}-coordinated glyme. Such a separation of $TFSI^-$ from the Mg^{2+} cations could explain the more facile Mg deposition in the measurements in Figure 1, but similar results could also be obtained from a weakening of the Mg^{2+}–$TFSI^-$ coordination. Finally, DFT calculations comparing the different abilities to coordinate cations in chloride-containing Mg complexes in monoglyme-, diglyme-, triglyme- and tetraglyme-based electrolytes indicated that the longer and more flexible glymes were increasingly able to adjust their conformation and thus enhance the interaction between Mg and solvent. This was proposed to allow for the formation of larger Mg^{2+}-, Cl^-- and solvent-containing aggregates, which, in turn, improves the reversibility of Mg deposition/dissolution, though at higher overpotentials.[60]

Focusing on BH_4^--containing electrolytes, both experimental studies[15,50] and calculations[61,62] for several electrolytes have concluded that the dissociation of the Mg^{2+}–BH_4^- coordination is a key aspect for Mg deposition, which, in ether-type solvents, is influenced by the number of coordinating oxygen atoms or possibly also by coordinating $TFSI^-$ ions. The Mg^{2+} coordination in BH_4^-- and $TFSI^-$-containing diglyme was investigated by Hu *et al.* in a combined experimental and theoretical study.[63] Using the electrolyte components without further purification or drying, they found an improved electrochemical performance in the mixed electrolyte as compared to a $TFSI^-$-free electrolyte. They explained this by a formation of mixed ion pair clusters containing Mg^{2+} as central ion, which is coordinated by BH_4^- and $TFSI^-$ anions as well as by O-atoms of the glyme molecules. The latter are expected to reduce the strong interaction between Mg^{2+} and BH_4^- anions, which was claimed to allow for reversible Mg plating and stripping.[63] Using a special $TFSI^-$-based IL with an oligoether group in the cation and $Mg(BH_4)_2$ as Mg source, Watkins *et al.* found that Mg deposition/dissolution reversibility are significantly improved compared to that from BMP-TFSI.[17] They attributed this to the complexation of the Mg^{2+} cation by the polyether groups, which prevents the direct $TFSI^-$ coordination and weakens the Mg^{2+}–BH_4^- coordination. Comparable results were reported by Gao *et al.*,[18] who, furthermore, observed that the above effects increase with increasing ether functionalization of the cation.

Based on aforementioned results, the crown ether may either displace the $TFSI^-$ anions from the Mg^{2+} coordination sphere and thus prevent the decomposition of the $TFSI^-$; or it may weaken the interaction with Mg^{2+} and thus stabilize the $TFSI^-$ against decomposition. In both cases, one would expect an improved reversibility of the Mg deposition/dissolution process and, in particular, a better stability/slower inhibition of these processes in the presence of the crown ether. Still open, however, is the role of the borohydride in this process. It may either solely act as water scavenger, removing trace impurities of water in the different chemicals (see Experimental section) from the electrolyte, or it may also coordinate to Mg^{2+}. BH_4^- coordination to Mg^{2+} has indeed been reported to be stronger than that of $TFSI^-$,[18,63] which will be important also for the present case. Finally, also the ratio between the different components seems to be important; as indicated by the results of Hu *et al.*, who observed significant differences in the Mg deposition/dissolution current when varying the ratio of the $TFSI^-$ and BH_4^- concentration in Mg^{2+}-containing diglyme.[63]

In order to investigate the role of the $TFSI^-$ and BH_4^- anions and of the crown ether and, in particular, their relative concentrations, in more detail, we prepared electrolytes with different concentrations of these species. In all cases, the Mg^{2+} concentration was kept at 0.1 mol L^{-1}. We would expect that, if borohydride acts only as water scavenger and is necessary for that, a certain minimum concentration of borohydride is required for reversible Mg deposition/dissolution. In that case, crown ether would be furthermore required to coordinate to Mg^{2+} and displace $TFSI^-$. Alternatively, both borohydride and crown ether contribute to the displacement of $TFSI^-$ from the Mg^{2+} coordination sphere. In this case, the total amount of

borohydride plus crown ether relative to the amount of Mg^{2+} would be decisive for reversible and reasonably stable Mg deposition/dissolution.

In Figure 2a, we present a set of CVs recorded with a GC substrate in $Mg(BH_4)_2$-, $MgTFSI_2$-, and 18-crown-6-containing BMP-TFSI, with a 1:1 molar ratio of crown ether to Mg^{2+} and a 1:1 mixture of $Mg(BH_4)_2$ and $MgTFSI_2$ (0.05 M $Mg(BH_4)_2$ + 0.05 M $MgTFSI_2$ + 0.1 M 18-crown-6). The characteristic features in these CVs are essentially identical to those obtained and discussed before for GC in a solution of 0.1 M $Mg(BH_4)_2$ and 0.1 M 18-crown-6 in IL (Figure 1). The reversibility is about 80% in the first ten cycles, which is comparable to the results obtained for the $MgTFSI_2$-free electrolyte (Figure 1). However, with increasing cycling times, the reversibility decreases to about 12% after 20 cycles (see Figure S6 and Table S3) and the electrode is completely inert after 50 cycles (Figure 2a). For comparison, the GC electrode cycled in BMP-TFSI + 0.1 M $Mg(BH_4)_2$ + 0.1 M 18-crown-6 (discussed with Figure 1) still displayed more than half of the initial current densities after 50 scans. Considering that the relative increase in $TFSI^-$ concentration is marginal and the concentrations of Mg^{2+} and 18-crown-6 are identical to those in Figure 1, these changes in reversibility must be related to the lower amount of BH_4^- in the measurement to Figure 2a.

Upon further increasing the amount of $MgTFSI_2$ at the expense of $Mg(BH_4)_2$ (Figure 2, 0.09 M $MgTFSI_2$ + 0.01 M $Mg(BH_4)_2$ + 0.1 M 18-crown-6), we observe a pronounced decay of the current density and a down-shift of the Mg deposition potential (blue curve). Obviously, the increasing lack of BH_4^- is detrimental for the Mg^{2+} deposition process. The current trace in the anodic scan is affected even more and shows only a very weak and broad Mg dissolution feature. Hence, both Mg plating and Mg stripping are reduced when replacing BH_4^- by $TFSI^-$, or the other way around, when reducing the amount of BH_4^-, while keeping the concentration of crown ether constant.

Interestingly, when doubling the amount of crown ether added to this $Mg(BH_4)_2/MgTFSI_2$ mixture (Figure 2b, violet dashed curve, 0.09 M $MgTFSI_2$ + 0.01 M $Mg(BH_4)_2$ + 0.2 M 18-crown-6, for more cycles see Figure S7 and Table S4), the high current densities are restored again and the reversibility is significantly improved. The latter increases from 75% in the first cycle to 82% in the second cycle, then decreases again continuously to 75% in the 10th cycle. This trend in the reversibility, with an initial increase and a later decrease, is very similar to that obtained for the sample cycled in IL containing 0.05 M $Mg(BH_4)_2$ + 0.05 M $MgTFSI_2$ + 0.1 M 18-crown-6 (Figure 2a). We assume that the similar trends reflect that, in both cases, an increasing excess of BH_4^- plus crown ether relative to the Mg concentration is beneficial for the Mg deposition/dissolution reaction. Also, the onset potential for Mg deposition (−0.6 V) is slightly more anodic than that obtained in pure borohydride and crown ether-containing IL with no $MgTFSI_2$ (−0.7 V, equivalent to an up-shift of the onset potential for Mg deposition by 0.1 V), supporting the above conclusion of more facile Mg deposition in this electrolyte. In combination, these results indicate that the sole coordination of $TFSI^-$ with Mg^{2+} is detrimental for the Mg deposition/dissolution processes. However, when either the crown ether or BH_4^- – or both in combination – are present in the electrolyte in sufficient amounts, $TFSI^-$ can either at least partly be displaced from the inner Mg^{2+} coordination sphere, or the Mg^{2+}–$TFSI^-$ interaction can be weakened to an extent that Mg^+-induced $TFSI^-$ decomposition is inhibited during reaction. Both could enable improved plating and stripping. On the other hand, Hu *et al.* had demonstrated that an increase of the $MgTFSI_2$ content, from zero content to fourfold excess at constant $Mg(BH_4)_2$ concentration (0.01 M), leads to a continuous increase in reversible Mg deposition/dissolution from diglyme.[63] Based on quantum chemical calculations, they proposed that $TFSI^-$ displaces one of the BH_4^- ligands in the inner coordination shell, which was seen as origin for the improved Mg deposition/dissolution. The apparent discrepancy to our findings – an improved Mg deposition/dissolution upon addition of $TFSI^-$ to $Mg(BH_4)_2$-containing electrolyte in their case vs. an improved Mg deposition performance upon addition of $Mg(BH_4)_2$ to $TFSI^-$-based electrolyte in our experiments – is most likely due to the very different situations in both cases. While in our

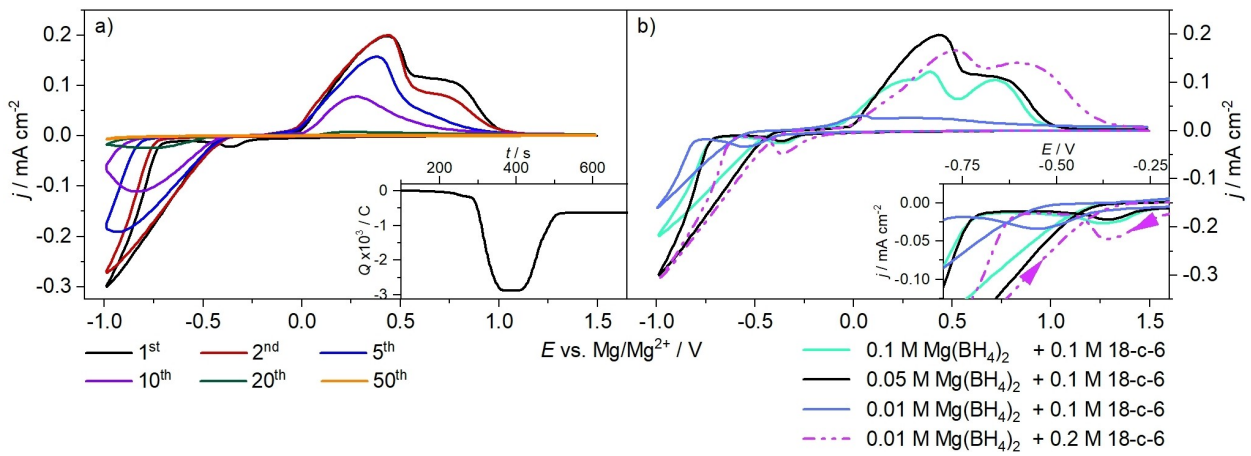

Figure 2. Sets of CVs recorded on GC in BMP-TFSI + 0.05 M $Mg(BH_4)_2$ + 0.05 M $MgTFSI_2$ + 0.1 M 18-crown-6 (a) and in BMP-TFSI with different concentrations of $Mg(BH_4)_2$, $MgTFSI_2$ and 18-crown-6 (b, first cycle). The concentration of $MgTFSI_2$ is 0.1 M – concentration of $Mg(BH_4)_2$. The inset in (a) shows the accumulated charge during the first scan, in (b) an enlarged section of the lower potential region between −0.2 and −0.8 V. All scan rates are 10 mV s^{-1}.

experiments $TFSI^-$ is present also as solvent and thus in strong excess, they use $TFSI^-$ in rather low concentrations, comparable to that of BH_4^-, together with an excess of the Mg-coordinating glyme as solvent.

These results point to an equilibrium of Mg^{2+} coordination with the various ligands, where coordination of $TFSI^-$ to Mg^{2+} and, thus, also Mg^+-induced decomposition of $TFSI^-$, are still possible as long as BH_4^- and/or crown ether (or a combination of them) are not present in over-stoichiometric amounts (for crown ether: 1:1). This conclusion also fits well to the results reported by Shao *et al.*, who observed a significant enhancement of the Coulombic efficiency with increasing BH_4^- concentration, as well as when changing from a monodentate solvent molecule (THF) to bidentate (DME) and finally tridentate (diglyme) molecules.[15] They explained this behavior by synergistic effects, without, however, explaining in more detail how this would affect Mg deposition. As mentioned before, we found that, also in the presence of crown ether, a certain amount of BH_4^- is required, as indicated by the experiment with 0.09 M $MgTFSI_2$ + 0.01 M $Mg(BH_4)_2$ + 0.1 M crown ether, where Mg deposition was strongly hindered. Finally, additional measurements with other concentrations of crown ether (Figure S3) further confirmed that a certain minimum amount of BH_4^- is required for Mg deposition from $MgTFSI_2$. Even a tenfold excess of crown ether did not support Mg deposition from $MgTFSI_2$ if no BH_4^- was added. This is most easily explained in a picture where some BH_4^- is necessary for removal of trace impurities of water, and, additionally may coordinate with Mg^{2+}.

Here it should be mentioned that Sagane *et al.* observed that the addition of stoichiometric (1:1) amounts of 18-crown-6 to $MgTFSI_2$ in MPPp–TFSI is required and sufficient for a complete displacement of $TFSI^-$ from the coordination sphere of the Mg^{2+}, resulting in the formation of "free" $TFSI^-$ anions. The CV of that mixture shows Mg plating and stripping, but with a very low reversibility.[42] Furthermore, there may be an influence of the IL cation on the complexation process, as these authors used 1-methyl-1-propylpiperidinium ($MPPp^+$) as cation rather than the 1-butyl-1-methyl-pyrrolidinium (BMP^+) employed in the present work.

Finally, we want to briefly test for possible effects induced by the nature of the electrode by changing to a Mg electrode. Figure 3 displays a CV recorded in 0.1 M $Mg(BH_4)_2$-containing BMP-TFSI with 0.1 M 18-crown-6 on a magnesium substrate. Different from the current traces recorded on the glassy carbon substrates in 0.1 M $Mg(BH_4)_2$ and 0.1 M 18-crown-6-containing IL, the first cathodic scan (after a potential step from the OCV to the upper potential limit) already exhibits oxidative currents in the potential range 1.5–0 V, which we assume are due to Mg dissolution from the roughened electrode (see Experimental section). This is different from results reported by Ma *et al.*, who only observed dissolution of freshly deposited Mg, but not of the Mg substrate, in 0.5 M $MgTFSI_2$/tetraglyme electrolyte containing 6 mM $Mg(BH_4)_2$, at least when cycling below 1.0 V. They concluded that, most likely, the underlying Mg surface is passivated completely despite the roughening pretreatment.[30] Mg deposition starts already at a potential below 0.5 V, i.e., at a

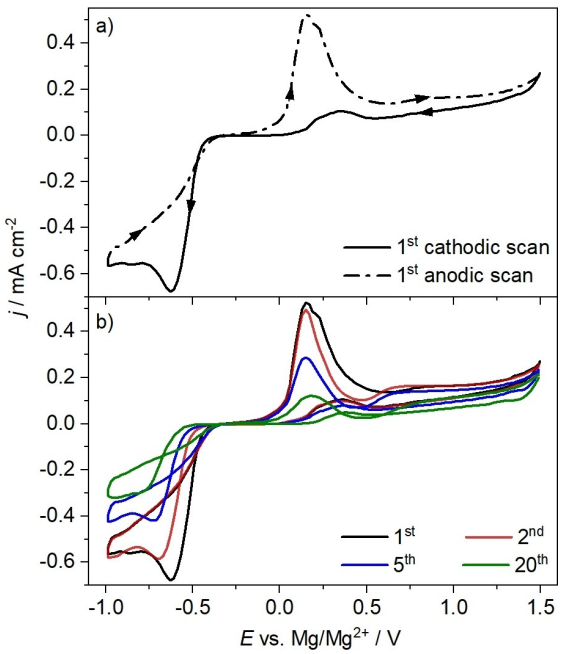

Figure 3. First (a) and additional relevant (b) cycles of the potentiodynamic scan of a Mg electrode in 0.1 M $Mg(BH_4)_2$ + 0.1 M 18-crown-6-containing BMP-TFSI at 10 mV s^{-1}.

lower overpotential compared to that obtained on a glassy carbon electrode in the same electrolyte (Figure 1, around 0.7 V). This indicates a lower nucleation overpotential for the roughened Mg electrode compared to the GC substrate, most likely due to the presence of efficient sites for heterogeneous nucleation on the surface. The corresponding Mg dissolution peak appears at 0.2 V, also down-shifted by 0.1 V compared to the Mg dissolution peak observed on GC. Initially, the current density is almost three times higher than the corresponding current traces on glassy carbon. With increasing cycle number it decreases rapidly, having lost about half the initial current density by the fifth cycle. This loss is far more pronounced than on glassy carbon. We tentatively explain this by the generally higher reactivity of the Mg surface, which reacts more efficiently both with trace impurities in the electrolyte and/or with the solvent during cycling. This reaction may hinder further Mg deposition and thus result in the distinct peak between −0.6 and −0.7 V in the Mg deposition range, rather than the expected exponential current increase when approaching the lower potential limit. The peak in the anodic scan at about 0.2 V is most likely related to dissolution of the freshly plated Mg, whereas oxidation of the underlying Mg substrate proceeds only in the anodic currents above 0.5 V. Interestingly, while the onset and peak maximum for Mg dissolution remain the same, the onset for Mg deposition shifts to more negative potentials with continued cycling. Overall, compared to Mg plating/stripping on GC, both these and also the passivation processes are faster on Mg.

It is also worth mentioning that, aside of its role as water scavenger, borohydride may also dissolve the (native) passivation layer present on the Mg surface due to its strongly

reducing nature.[14] However, we observed both Mg deposition/dissolution and electrolyte decomposition currents only on *in situ* roughened Mg electrodes. Hence, the sole presence of borohydride is not enough to dissolve the native passivation layer and allow for reversible Mg plating and stripping.

To learn more about the question in how far these effects are specific for Mg deposition, we studied the plating/stripping behavior on GC in analogous electrolyte systems, employing Ca^{2+} instead of Mg^{2+}. No Ca^{2+} deposition was observed from $Ca(BH_4)_2$-containing BMP-TFSI, neither in the absence nor presence of 18-crown-6 (Figure S2 and S3). We speculate that this difference is related to the different mismatch[49] between the cavity size of the crown ether (2.9 Å for 18-crown-6) and the ion diameters of the two ions (Ca^{2+} 2.0 Å, Mg^{2+} 1.44 Å). The better fit would result in a stronger binding of Ca^{2+} than of Mg^{2+}. In that case, Mg^{2+} deposition could still be possible when it is coordinated to 18-crown-6, while Ca^{2+} is too tightly bound for deposition. This hypothesis is also in agreement with the fact that we found neither Ca nor Mg deposition from BMP-TFSI containing 15-crown-5 (cavity size 2.0 Å), as, as we assume, both cations are too strongly bound for metal deposition.

Finally, we would like to note that the proposed mechanism of a displacement of the anion of the IL solvent/Mg source by the additives requires that the additives coordinate more strongly to the Mg^{2+} cation than the weakly coordinating $TFSI^-$ anions and also weaken the Mg^{2+}–$TFSI^-$ interaction, but still are sufficiently weakly coordinated to allow facile Mg deposition. The partial displacement of the Mg^{2+}-coordinated $TFSI^-$ species and the weakening of the Mg^{2+}–$TFSI^-$ interaction of the remaining $TFSI^-$ ligands inhibits the decomposition of the $TFSI^-$, which is induced by interaction with the Mg^+ upon partial reduction of the Mg^{2+} ion.[28] Hence, we propose that in such cases the optimum additive is one that is i) stable against decomposition itself and that has ii) an optimum interaction with the metal cation; i.e., sufficiently strong that it can partly displace the instable component (here $TFSI^-$) and/or weaken its interaction with the central Mg^{2+} ion, but sufficiently weak that it does not inhibit metal deposition by formation of a stable coordination shell. This also requires that the coordination of the unstable component be sufficiently weak that it can still be displaced by the additive under the conditions described in ii). These questions were investigated theoretically, as detailed in the next section.

2.2. Simulation

To test the above interpretation, we conducted MD simulations and quantum chemical calculations at the density functional level of theory (DFT), comparing the stability of the coordination sphere of the Mg^{2+} cation in the presence and absence of 18-crown-6 (for details, see Experimental section and Supporting Information). Note that in our classical MD simulations, which are used as starting point, the interactions between Mg^{2+} and the solvent molecules are limited to solely electrostatic forces and will not include contributions from covalent interactions between Mg^{2+} and oxygen. However, such interactions are fully captured in the subsequent DFT calculations. In these calculations, the reference level for the energy of the respective clusters was defined by the energy of an isolated $MgTFSI_2$ cluster plus that of the separate additional ligands (BMP-TFSI ion pairs, 18-crown-6), where the energies were calculated using the frozen geometry of the most stable complete cluster. Accordingly, the coordination energies E_c refer to the energy gained upon coordinating one or more additional ligands to the $MgTFSI_2$ cluster, while the binding energy E_b of a specific ligand in that cluster refers to the energy required for removing that ligand in a frozen configuration. For selected configurations obtained during the MD simulations, we cut clusters containing the $MgTFSI_2$ as well as up to two BMP-TFSI ion pairs in the absence and presence of 18-crown-6, which were further optimized geometrically (see Experimental section). For the determination of the coordination and binding energies presented in Figures 4 and 6 and in Table 1, we used the cluster configurations with the most stable final geometry. Note that the structure of the $MgTFSI_2$ complex included therein may not be the most stable configuration of the isolated $MgTFSI_2$ cluster.

In Figure 4, we show a selection of clusters cut from the MD simulations consisting of $MgTFSI_2$ in the presence of up to two BMP-TFSI ion pairs and up to one 18-crown-6 molecule. The Mg^{2+} cation is displayed in different coordination states and geometries, along with the respective (additional) coordination energies. The clusters are portrayed in the most stable configurations observed for the respective coordination. Note that these are not necessarily the configurations with the highest coordination energies. Visualizations of some other clusters considered in this work are provided in the Supporting Information (Figure S8). A main characteristic for all clusters is the bond between the Mg^{2+} cation and the oxygen atoms of the $TFSI^-$ anions or of the 18-crown-6 molecule. The different configurations in Figure 4 involve coordination geometries of the Mg^{2+} cation with different numbers of directly coordinating oxygen atoms, as illustrated in Figure 5. The Mg^{2+} cation prefers a seven-fold coordination by oxygen atoms in the presence of 18-crown-6, while a five- or six-fold oxygen coordination, arranged in a pyramidal or octahedral configuration, respectively, is preferred in its absence.

As expected, the increasing coordination of the Mg^{2+} ion in the $MgTFSI_2$ cluster increases the stability of the cluster. Coordination with an additional BMP-TFSI ion pair leads to a stabilization by −132 kJ/mol (Figure 4a). Note that this denotes

Table 1. Electron affinity E_A and equilibrium potential E_{red} for molecule/cluster reduction vs. Mg/Mg^{2+} for different molecule/cluster types.

Cluster/molecule	E_A [eV]	E_{red} [V]
$TFSI^-$	2.16	−1.19
18c6	−0.49	−3.84
Mg^{2+} + 18c6	1.68	−1.67
$MgTFSI_2$	3.75	0.40
$MgTFSI_2$ + BMP-TFSI	3.49	0.14
$MgTFSI_2$ + 2 BMP-TFSI	3.10	−0.25
$MgTFSI_2$ + 18c6	2.97	−0.38
$MgTFSI_2$ + 18c6 + BMP-TFSI	2.91	−0.44

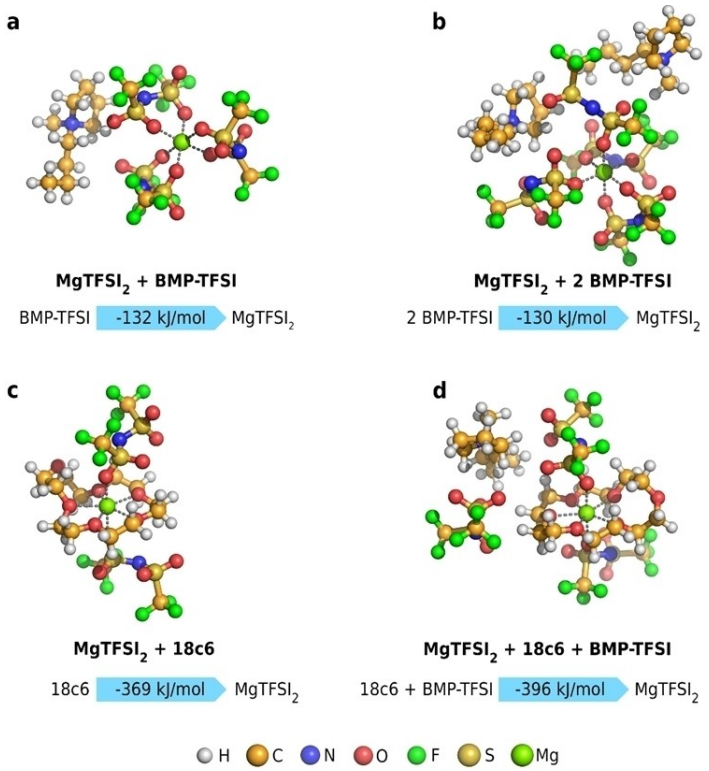

Figure 4. Representation of the most stable clusters at different compositions, cut from MD simulations, and the respective coordination energies E_c.

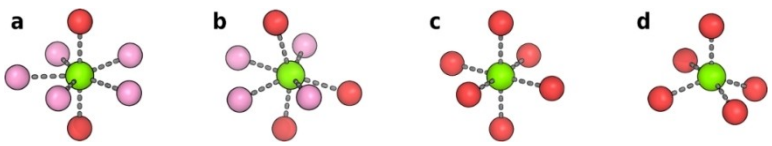

Figure 5. Different coordination states of Mg^{2+}, colored in green, in the presence (a, b) and absence (c, d) of 18-crown-6. Oxygen atoms belonging to the 18-crown-6 ring are colored in pink; those belonging to $TFSI^-$ in red.

the overall energy gain of the system, which may also contain contributions from a change in bonding within the original $MgTFSI_2$ cluster and within the ion pair. Hence, it is not necessarily the strength of the bond between Mg^{2+} and the ion pair, but it would properly describe the energy needed to detach the ion pair. Adding a second BMP-TFSI ion pair to the $MgTFSI_2$ + BMP-TFSI cluster does not lead to a further stabilization of the cluster; the coordination energy of −130 kJ/mol for two BMP-TFSI ion pairs is almost equal to that of a single ion pair (Figure 4b). Qualitatively, this can be understood from the fact that, for coordination with a single BMP-TFSI ion pair, the $TFSI^-$ anion can coordinate via two oxygen atoms, while for coordination by two BMP-TFSI ion pairs each of them coordinates only by a single oxygen atom of the $TFSI^-$ species to the Mg^{2+} cation (see Figure 4). Hence, coordination by the second ion pair weakens the bond to the first ion pair, and this effect is quite significant. Therefore, one would expect an equilibrium between both states at room temperature, which also means that thermal detachment of the second ion pair is easily achieved at room temperature. This weakening of the bond to the first BMP-TFSI ion pair is illustrated also in the energy scheme in Figure 6. It represents the binding energies for different ligands in the frozen geometry of the final cluster, which were calculated by comparing the cluster energies before and after removal of the respective ligand in that geometry. In this case, the binding energies of the two different BMP-TFSI ion pairs are almost identical (Figure 6c), and they are much smaller than that of the BMP-TFSI ion pair in Figure 4a. Also, it does not seem to matter which of the two ion pairs is added first. Hence, synergistic effects between the two ion pairs are absent.

In a similar way, we explored the additional coordination of an 18-crown-6 molecule to either the $MgTFSI_2$ (Figure 4c) or the $MgTFSI_2$ + BMP-TFSI (Figure 4d) cluster. In the first case, this results in a stabilization by −369 kJ/mol. Hence, the coordination of the $MgTFSI_2$ cluster by the crown ether is significantly stronger than that by a BMP-TFSI ion pair. Also, the addition of a single 18-crown-6 molecule to a $MgTFSI_2$ + BMP-TFSI cluster results in a drastic increase in cluster stability by −264 kJ/mol. Qualitatively, this is evident already from the structure of the most stable cluster in Figure 4d. This shows a significant weakening of the coordination to the two original $TFSI^-$ anions,

which are coordinated now only via one oxygen atom, and to the third $TFSI^-$ anion (that of the BMP-TFSI ion pair), which is no longer part of the inner coordination sphere. Here, we identify the $TFSI^-$ anion of the ion pair by its stronger interaction to the BMP^+ cation compared to the other two $TFSI^-$ species. On a more quantitative scale, this is illustrated in the energy scheme in Figure 6d. Addition of a crown ether molecule to the $MgTFSI_2$ cluster, in the frozen geometry of the stable configuration of the $MgTFSI_2$ + BMP-TFSI + 18-crown-6, results in a binding energy stabilization by −353 kJ/mol; further addition of a BMP-TFSI ion pair stabilizes this by another −43 kJ/mol (total coordination energy −396 kJ/mol), which is even less than the binding energy per BMP-TFSI ion pair in the $MgTFSI_2$ + BMP-TFSI cluster. Also in this case, it almost does not matter whether the crown ether or the ion pair is added first and synergies are very small. Overall, the strong coordination by the crown ether molecule leads to a significant weakening of the bond between Mg^{2+} and the two $TFSI^-$ anions, and essentially a displacement of the BMP-TFSI ion pair. Also considering these effects in the overall energy balance, one expects that the bond between crown ether and Mg^{2+} cation is even significantly stronger than −353 kJ/mol.

In addition to the above calculations, we also explored whether coordination of two 18-crown-6 molecules to the $MgTFSI_2$ cluster would be strong enough to additionally displace the original $TFSI^-$ anions from their direct coordination to the Mg^{2+} cation. For this purpose, we built and optimized a cluster in which the Mg^{2+} cation is surrounded by two 18-crown-6 molecules and the two $TFSI^-$ anions are displaced to the second coordination layer (Figure S9). Here, we find that the total binding energy in that cluster is stronger by −70 kJ/mol, as compared to the coordination states in the absence of 18-crown-6. However, it is less stable by −27 kJ/mol as compared to the coordination by just one 18-crown-6 and two directly coordinating $TFSI^-$ anions.

Overall, these calculations indicate that i) the coordination with the 18-crown-6 molecule is much stronger than that with $TFSI^-$ anions, that ii) the interaction with the 18-crown-6 molecule leads to a significant destabilization of the remaining coordination to the two $TFSI^-$ anions, as indicated by the change from two-fold to one-fold coordination, and, finally, that iii) a complete screening of the Mg^{2+} cation by two 18-crown-6 molecules is energetically unfavorable. In the absence of 18-crown-6, the coordination of $MgTFSI_2$ with one or two BMP-TFSI ion pairs always results in either a six-fold or five-fold coordination of the Mg^{2+} cation, i.e., in an octahedral or trigonal bipyramidal structure, respectively. In contrast, in the presence of 18-crown-6, the Mg^{2+} cation is coordinated by four to five oxygen atoms of the ether and two to three anions coordinated by a single oxygen atom each.

Next, we considered that Mg deposition requires the cation to be able to (stepwise) strip its coordination shell when attaching to the electrode surface. As evident from the numbers in Figures 4 and 5, the binding energies with the $TFSI^-$ anions in the BMP-TFSI ion pairs calculated are of an order of magnitude that allows their thermal detachment at room temperature. This is true both for coordination of one or two ions pairs – actually, removing the second BMP-TFSI ion pair does not cost any energy – and especially in the presence of a crown ether molecule acting as a second ligand. On the other hand, it would be very hard for the Mg^{2+} cation to escape coordination with 18-crown-6. Previous studies have suggested that the partial reduction of Mg^{2+} to Mg^+ via an outer sphere electron transfer reaction will weaken the interaction with $TFSI^-$.[18,28] Similar effects may also be expected for the coordination to an 18-crown-6 molecule. Figure 7 compares the coordination energies of different 18-crown-6 and/or BMP-TFSI-containing clusters before and after partial reduction of the cation from Mg^{2+} to Mg^+. Indeed, the coordination energies decrease significantly (strictly speaking, the absolute values of the coordination energies decrease). Most importantly, the coordination energy of the 18-crown-6-containing cluster decreases by −130 kJ/mol, falling to −212 kJ/mol. This moves it significantly closer to the range where Mg deposition seems feasible. On the other hand, while the addition of a second BMP-TFSI ion pair to the coordination sphere of Mg^{2+} does not result in a further stabilization of the cluster (see above), this is different for the reduced Mg^+ ion. Here, the addition of a second BMP-TFSI ion pair to the coordination sphere of $[MgTFSI_2]^-$ reduces the cluster stability, which, in turn, would improve Mg deposition on the electrode due to its reduced coordination. Overall, the data in Figure 7 demonstrate that

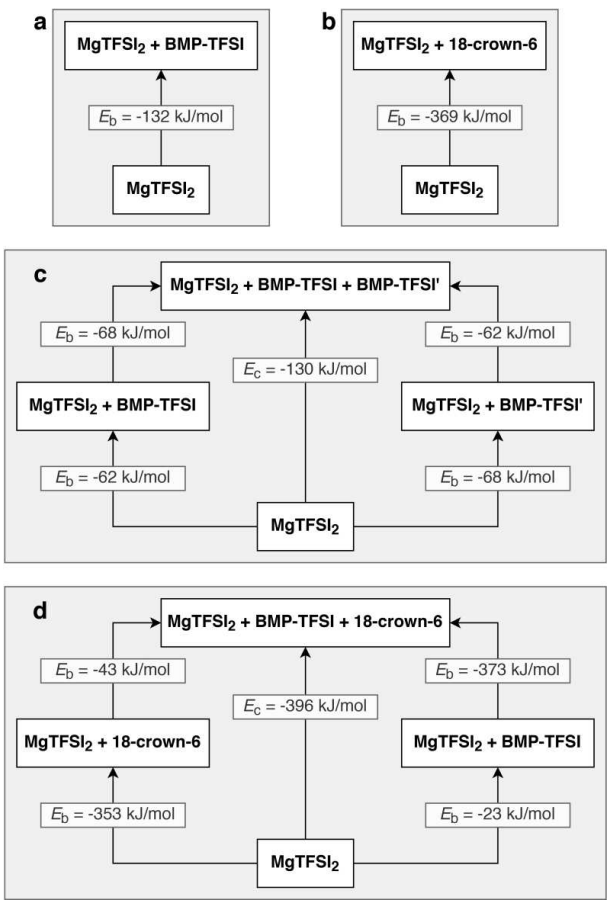

Figure 6. Scheme of the coordination energies E_c and binding energies E_b for different cluster compositions.

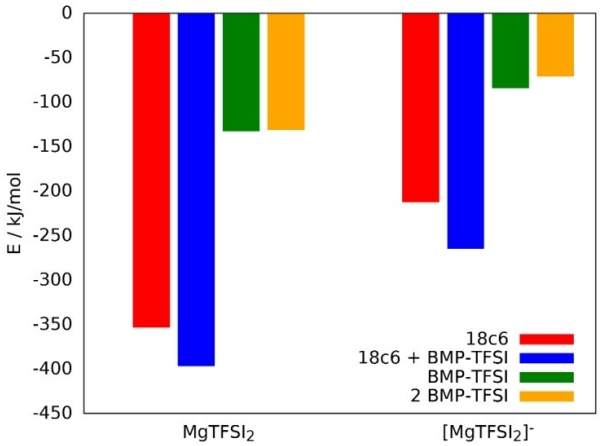

Figure 7. Coordination energies of different 18-crown-6 and BMP-TFSI-containing clusters ($MgTFSI_2$ + X, X see Figure) with [Mg^{2+}—$TFSI_2$] or [Mg^{+}—$TFSI_2$]$^{-}$ as central unit. Coordination energies are referenced to the energies of the respective $MgTFSI_2$ clusters.

partial reduction of the Mg^{2+} to Mg^{+}, e.g., via an outer sphere charge-transfer step, destabilizes the coordination not only to solvent ion pairs, but also to 18-crown-6 molecules to an extent that detachment of these species becomes feasible at room temperature, which is a precondition for Mg deposition.

Finally, we investigated the reductive stability of the $TFSI^{-}$ anions in different clusters. Recently, several groups have proposed to derive trends in the electrochemical stability window calculating reduction and oxidation potentials, rather than using the strongly simplified previous scheme which relates the stability window to the HOMO and LUMO of the solvent molecules.[64–67] The main difference in this approach is the proper accounting of solvation effects and of contributions from reduction-/oxidation-induced reactions.[67] Here, we employed a method which is closely related to the general ideas of the thermodynamic cycle method, but proceeds in a different way: namely, by calculating the electron affinities E_A of the solvated clusters based on the adiabatic energy difference between a cluster and its reduced form. As described in the Experimental section, both clusters were geometry-relaxed to the nearest local minimum. Table 1 lists the values of E_A for a number of different clusters. For comparison, we also included the isolated $TFSI^{-}$ anion, the 18-crown-6 molecule, and the $MgTFSI_2$ cluster. Based on the electron affinities, trends in the equilibrium potential for reduction of the respective molecules/cluster E_{red} can be estimated (see Experimental section), which are listed in Table 1 as well.

First of all, we find that the uncoordinated $TFSI^{-}$ anion shows a significantly higher electron affinity compared to its coordinated state in the $MgTFSI_2$ cluster. Considering the magnitude of the difference in electron affinities, this trend is significant, even though for these latter two species solvation effects are included only implicitly. A similar trend can be observed for 18-crown-6, which becomes more susceptible to reduction when coordinated to Mg^{2+}. However, both in its free and its coordinated state, 18-crown-6 ether shows significantly lower electron affinities than $TFSI^{-}$.

Furthermore, we found that, during geometric relaxation, all $TFSI^{-}$-containing clusters exhibit the dissociation of a $-CF_3$ group upon reduction. Therefore, the electron affinity of the $TFSI^{-}$-containing clusters is a measure also for the stability against reductive decomposition of the $TFSI^{-}$ group. In contrast, no bond breaking was observed in the 18-crown-6 ether, neither in the free molecule nor when coordinated to Mg^{2+} or $MgTFSI_2$. Spin density plots (Figure S15) reveal that, in $TFSI^{-}$-containing clusters, the unpaired electron is entirely located on the dissociated $-CF_3$ group after reduction, whereas in the case of the isolated $TFSI^{-}$ the unpaired electron is shared between both fragments. In the absence of $TFSI^{-}$ and presence of 18-crown-6, the additional, unpaired electron will be entirely located at the Mg^{2+} cation, reducing it to Mg^{+}. Hence, the coordination to Mg^{2+} strongly enhances the known tendency of $TFSI^{-}$ to decompose upon reduction via dissociation of a $-CF_3$ group.[18,28,68] Similar findings were recently described by Tuerxun *et al.* for $MgTFSI_2$ in different organic solvents (THF, diglyme), based on the comparison of the calculated HOMO/LUMO energy levels of the free $TFSI^{-}$ and of the $MgTFSI_2$ cluster, respectively.[20] In this case, implicit solvation effects were included, while explicit solvent effects by coordination of solvent molecules were not considered. Furthermore, we found that the addition of one BMP-TFSI ion pair slightly reduces the electron affinity E_A. On the other hand, the reductive stability of the coordinated $TFSI^{-}$ anion is significantly increased by the addition of an 18-crown-6 ligand. Hence, even though there are still two $TFSI^{-}$ anions weakly coordinated to the Mg^{2+} cation also in the presence of the 18-crown-6 molecule, these are less susceptible to reductive decomposition than the strongly coordinated $TFSI^{-}$ species present in the absence of the crown ether. The same trend is indicated by the spin density distribution plots. A high electron affinity correlates with a pronounced localization of the unpaired electron, whereas the clusters with lower electron affinity show a more diffuse spin distribution. In isolated 18-crown-6, the electron is delocalized over the whole ring upon reduction, while the additional electron is localized on the cation upon attachment to Mg^{2+}, reducing it to Mg^{+} and increasing the electron affinity. The reduction of isolated $TFSI^{-}$ leads to the dissociation of a $-CF_3$ group, but the spin density plot shows that the unpaired electron is still shared between both fragments in the stable configuration. Again, the interaction with Mg^{2+} leads to a pronounced localization of the electron, which is then entirely located on the dissociated $-CF_3$ group. This leaves the other fragment with a twofold negative charge, which is stabilized by the cation. In the presence of 18-crown-6, the spin density distribution becomes more diffuse again, which goes along with a lower electron affinity.

Overall, on a qualitative scale these calculations can well explain the experimental observation that i) the addition of 18-crown-6 results in a pronounced suppression of the reductive decomposition of $TFSI^{-}$ species, even though these are present at large excess, and that ii) Mg^{2+} deposition is still possible despite the rather strong coordination of the 18-crown-6 molecule to the Mg^{2+} cation. In the first case, this is due to the fact that coordination to 18-crown-6 prohibits the two-fold

coordination to the $TFSI^-$ anions and, thus, decreases their binding energy to the Mg^{2+} cation. On the other hand, for the partly reduced Mg^+, the interaction of the 18-crown-6 additive with the Mg^+ cation is sufficiently weak that direct interaction with the electrode as a first step for Mg deposition seems to be feasible at room temperature.

3. Conclusions

Based on the results of a systematic electrochemical and theoretical study on the influence of additives, in our case 18-crown-6 and $Mg(BH_4)_2$, on the reversible deposition/dissolution of Mg on a glassy carbon model electrode in the ionic liquid BMP-TFSI, we could show that these can significantly improve the extent and reversibility of Mg plating/stripping. While Mg^{2+} deposition is inhibited in purely $MgTFSI_2$-containing BMP-TFSI, it is improved upon addition of the crown ether and/or of $Mg(BH_4)_2$. Varying the amount of the additives while keeping the Mg^{2+} concentration constant reveals i) that either of them can improve the deposition characteristics. However, ii) a certain excess of these species together relative to the Mg^{2+} concentration is required for more facile and reversible Mg deposition, and iii) regardless of the presence of the crown ether, a minimum amount of BH_4^- is required as well, most likely to act as water scavenger. These trends can be convincingly explained by the results of our quantum chemical calculations. Including implicit and explicit solvent effects, they reveal that i) the interaction between Mg^{2+} and the surrounding $TFSI^-$ anions is significantly weakened upon coordination of an 18-crown-6 molecule to $MgTFSI_2$ or to $MgTFSI_2$ + BMP-TFSI, which severely reduces the tendency for Mg^+-induced $TFSI^-$ decomposition during Mg^{2+} reduction, that ii) increasing coordination stabilizes the resulting cluster, but with a non-linear effect, that iii) partial reduction of Mg^{2+} to Mg^+, possibly via an outer sphere reduction process, weakens the $[Mg^+ - TFSI_2]^-$ interaction, which allows for coordination of the Mg cation to the electrode at room temperature, and that iv) the changes in Mg–TFSI interaction are reflected also by changes in the electron affinity and in the equilibrium potential for reduction of the respective clusters. When using a Mg substrate, as common in realistic battery systems, instead of the model GC electrode, the passivation process is far more efficient, but otherwise the data appear to be in agreement with our interpretation.

In combination, experiment and calculations result in a detailed mechanistic picture of the role of additives on Mg deposition/dissolution in an ionic liquid electrolyte, including also synergistic effects. The observation of similar trends for reversible Mg plating/stripping on GC model electrodes and realistic Mg electrodes, only with higher currents, indicates that the above picture is not electrode-specific, but of more general validity.

Experimental Section

Electrochemical Methods

For the preparation of the electrolytes, the appropriate amounts of $Mg(BH_4)_2$ (Sigma Aldrich, 95.0%), $MgTFSI_2$ (Solvionic, 99.5%, $\leq$250 ppm H_2O) and 18-crown-6 (Alfa Aesar, 99.0+%, $\leq$0.29% H_2O) were dissolved in 1-butyl-1-methylpyrrolidinium bis(trifluoromethylsulfonyl)imide (BMP-TFSI, Solvionic, 99.9%, $\leq$20 ppm H_2O) by stirring. We prepared the following solutions: BMP-TFSI with a) 0.1 M $Mg(BH_4)_2$, b) 0.1 M $Mg(BH_4)_2$ + 0.1 M 18-crown-6, c) 0.05 M $Mg(BH_4)_2$ + 0.05 M $MgTFSI_2$ + 0.1 M 18-crown-6, d) 0.01 M $Mg(BH_4)_2$ + 0.09 M $MgTFSI_2$ + 0.1 M 18-crown-6, and e) 0.01 M $Mg(BH_4)_2$ + 0.09 M $MgTFSI_2$ + 0.2 M 18-crown-6. Karl Fischer Titration of solutions of 0.1 M $MgTFSI_2$ + BMP-TFSI and 0.1 M $MgTFSI_2$ + 0.1 M 18-crown-6 in BMP-TFSI yielded water contents of 23 and 35 ppm, respectively. The water content of $Mg(BH_4)_2$-containing solutions cannot be determined this way due to its reaction with iodide; here we assumed similar water contents in the solvent and that all water originally present in the $Mg(BH_4)_2$-containing electrolyte was reactively removed. Electrochemical measurements were conducted in a beaker cell-type three-electrode setup using glassy carbon (GC, HTW Germany, Sigradur G, 4 mm thickness, d = 8 mm) or Mg disks (Goodfellow, 1.5 mm thickness, d = 8 mm, 99.9%) as working electrode (WE), a gold wire as counter electrode (CE) and a Mg rod (Goodfellow, d = 3.2 mm, 99.9%) as quasi-reference electrode (RE).

The electrochemical cell consists of a KelF cell body with three interconnected compartments and a total volume of 0.7 ml. CE and RE are placed in the outermost and middle compartment, respectively. With this configuration, the distance between counter and working electrode is maximized to minimize effects of oxidative reaction products formed at the CE on the processes taking place at the WE. The WE compartment, finally, has an opening at the bottom, with the edges of the opening pressing on the WE. A Viton O-ring (FKM 75, inner diameter 5 mm, cross section 1 mm) between WE and cell body prevents electrolyte leakage. Prior to the assembly, the GC substrates were polished and rinsed with Caroic acid, acetone, and ultrapure water. The cell body and O-rings were rinsed with acetone and then sonicated and boiled in ultrapure water. All cell components were finally dried in Ar atmosphere at 100 °C for 16 hrs. The Mg electrodes (both reference and working electrodes) were polished in an Ar-filled glove box (MBraun LabStar, $O_2 < 0.5$ ppm; $H_2O < 1$ ppm) before use. The cell was assembled inside the glove box, then quickly filled with electrolyte. In addition, the Mg electrode was roughened immediately after electrolyte filling, using a sharp glass tip. The potential was controlled by a Solartron Analytical Modulab (Pstat 1MS/s) potentiostat. Cycling involved at least 25 and at maximum 100 cycles between 1.5 and −1.0 V vs. Mg/Mg^{2+} at 10 mV s^{-1}. The electrochemical measurements were always started with a potential step from the OCV to the upper potential limit, with a rest time of 60 s at that point before the CV was initiated with the cathodic scan.

Computational Methods

Classical molecular dynamics (MD) simulations of $MgTFSI_2$ in BMP-TFSI in the presence and absence of 18-crown-6 were performed using the LAMMPS program package (version 17th of Nov, 2016),[69] employing the OPLSA-AA force field[70] for Mg^{2+} and 18-crown-6 and the CL&P force field for the ionic liquid (BMP-TFSI).[71] In these simulations, the solvent was represented by 256 BMP-TFSI ion pairs. For selected compositions, clusters were cut from these simulations using the post-processing tool TRAVIS.[72,73] The cluster structures

were geometrically optimized to the local energy minimum using density functional theory (DFT) with the ORCA program package,[74] the BP86 functional[75,76] and def2-SVP[77] basis set with Grimme's D3 dispersion correction.[78] Geometrical counterpoise (gCP) correction was applied to deal with the inter-molecular as well as intra-molecular basis set superposition error (BSSE).[79] Tight SCF convergence criteria were applied in each geometry optimization. Solvent effects were considered via the MD simulation; furthermore, they were considered explicitly in the DFT calculations by BMP-TFSI ion pairs in the cluster and implicitly by the conductor-like polarizable continuum model (CPCM);[80] setting the dielectric constant to 14.7[81] and the refractive index to 1.423.[82] Note that, while electrostatic interactions are the dominant attractive force between Mg^{2+} and oxygen, covalent interactions may also contribute to this, leading to delocalization of electron density to the cation's empty 3s and 3p orbitals. Such effects are not included in our classical MD simulations, which serve as starting point, but are fully considered in the subsequent DFT optimizations. Cluster coordination energies and ligand binding energies were obtained by performing single-point calculations of isolated parts of the optimized clusters at the same level of theory, maintaining their frozen structure (see also Results – Simulation). Electron affinities E_A and the equilibrium potential for reduction E_{red} of the respective clusters were obtained by explicitly calculating the adiabatic energy difference between a cluster R and its reduced form R^- (all geometry-optimized) via Equation (1):

$$E_A(R) = E(R) - E(R^-) \quad (1)$$

and Equation (2):

$$E_{red}(R) = \frac{E_A(R)}{nF} - E_{ref} \quad (2)$$

where $E(R)$ and $E(R^-)$ are the electronic energies of the solvated clusters, n is the number of exchanged electrons, F is the Faraday constant and E_{ref} is the reference potential calculated for Mg/Mg^{2+}. This yields values very close to those obtained by via the thermodynamic cycle method.[64–67]

Acknowledgements

We would like to thank Dr. Markus Eckardt and Sascha Gehrke for their help with the electrochemical pre-tests and MD simulations, respectively. We gratefully acknowledge financial support by the German Federal Ministry of Education and Research (BMBF) in the project 03EK3051 C ('LuCaMag: Wege zu sekundären Mg/Ca–Luftbatterien') and by the Deutsche Forschungsgemeinschaft under project BE 1201/22-1 ('Zn-Air Batteries') and ID 422053626 (POLiS Cluster of Excellence). This work contributes to the research performed at CELEST (Center for Electrochemical Energy Storage Ulm-Karlsruhe). Open access funding enabled and organized by Projekt DEAL.

Conflict of Interest

The authors declare no conflict of interest.

Keywords: magnesium batteries · magnesium · complexing additives · electrochemistry · quantum chemical calculations

[1] P. Novák, F. Joho, R. Imhof, J. C. Panitz, O. Haas, *J. Power Sources* **1999**, *81*, 212–216.
[2] D. Aurbach, Y. Gofer, A. Schechter, O. Chusid, H. Gizbar, Y. Cohen, M. Moshkovich, R. Turgeman, *J. Power Sources* **2001**, *97*, 269–273.
[3] I. Shterenberg, M. Salama, Y. Gofer, E. Levi, D. Aurbach, *MRS Bull.* **2014**, *39*, 453–460.
[4] R. Mohtadi, F. Mizuno, *Beilstein J. Nanotechnol.* **2014**, *5*, 1291.
[5] C. B. Bucur, T. Gregory, A. G. Oliver, J. Muldoon, *J. Phys. Chem. Lett.* **2015**, *6*, 3578–3591.
[6] Z. Zhao-Karger, M. Fichtner, *MRS Commun.* **2017**, *7*, 770–784.
[7] N. N. Rajput, T. J. Seguin, B. M. Wood, X. Qu, K. A. Persson, *Top. Curr. Chem. (Z)* **2018**, *376*, 19.
[8] M. Fichtner, *Magnesium Batteries: Research and Applications*, The Royal Society of Chemistry **2020**; Chapter 1, pp. 1–16.
[9] Z. Lu, A. Schechter, M. Moshkovich, D. Aurbach, *J. Electroanal. Chem.* **1999**, *466*, 203–217.
[10] T. S. Arthur, P. A. Glans, N. Singh, O. Tutusaus, K. Nie, Y. S. Liu, F. Mizuno, J. Guo, D. H. Alsem, N. J. Salmon, R. Mohtadi, *Chem. Mater.* **2017**, *29*, 7183–7188.
[11] T. Gao, S. Hou, K. Huynh, F. Wang, N. Eidson, X. Fan, F. Han, C. Luo, M. Mao, X. Li, *ACS Appl. Mater. Interfaces.* **2018**, *10*, 14767–14776.
[12] R. Lv, X. Guan, J. Zhang, Y. Xia, J. Luo, *Nat. Sci. Rev.* **2019**, *7*, 333–341.
[13] J. H. Connor, W. E. Reid, G. B. Wood, *J. Electrochem. Soc.* **1957**, *104*, 38–41.
[14] R. Mohtadi, M. Matsui, T. S. Arthur, S. J. Hwang, *Angew. Chem. Int. Ed.* **2012**, *51*, 9780–9783; *Angew. Chem.* **2012**, *124*, 9918–9921.
[15] Y. Shao, T. Liu, G. Li, M. Gu, Z. Nie, M. Engelhard, J. Xiao, D. Lv, C. Wang, J. G. Zhang, *Sci. Rep.* **2013**, *3*, 3130.
[16] M. Kar, Z. Ma, L. M. Azofra, K. Chen, M. Forsyth, D. R. MacFarlane, *Chem. Commun.* **2016**, *52*, 4033–4036.
[17] T. Watkins, A. Kumar, D. A. Buttry, *J. Am. Chem. Soc.* **2016**, *138*, 641–650.
[18] X. Gao, A. Mariani, S. Jeong, X. Liu, X. Dou, M. Ding, A. Moretti, S. Passerini, *J. Power Sources* **2019**, *423*, 52–59.
[19] Z. Ma, M. Forsyth, D. R. MacFarlane, M. Kar, *Green Energy & Environ.* **2019**, *4*, 146–153; Environ. **2019**, 4, 146–153.
[20] F. Tuerxun, K. Yamamoto, M. Hattori, T. Mandai, K. Nakanishi, A. Choudhary, Y. Tateyama, K. Sodeyama, A. Nakao, T. Uchiyama, M. Matsui, K. Tsuruta, Y. Tamenori, K. Kanamura, Y. Uchimoto, *ACS Appl. Mater. Interfaces* **2020**, *12*, 25775–25785.
[21] S. Y. Ha, Y. W. Lee, S. W. Woo, B. Koo, J. S. Kim, J. Cho, K. T. Lee, N. S. Choi, *ACS Appl. Mater. Interfaces* **2014**, *6*, 4063–4073.
[22] C. J. Barile, R. Spatney, K. R. Zavadil, A. A. Gewirth, *J. Phys. Chem. C* **2014**, *118*, 10694–10699.
[23] T. Fukutsuka, K. Asaka, A. Inoo, R. Yasui, K. Miyazaki, T. Abe, K. Nishio, Y. Uchimoto, *Chem. Lett.* **2014**, *43*, 1788–1790.
[24] N. Sa, N. N. Rajput, H. Wang, B. Key, M. Ferrandon, V. Srinivasan, K. A. Persson, A. K. Burrell, J. T. Vaughey, *RSC Adv.* **2016**, *6*, 113663–113670.
[25] S. Terada, T. Mandai, S. Suzuki, S. Tsuzuki, K. Watanabe, Y. Kamei, K. Ueno, K. Dokko, M. Watanabe, *J. Phys. Chem. C* **2016**, *120*, 1353–1365.
[26] S. Hebié, F. Alloin, C. Iojoiu, R. Berthelot, J. C. Leprêtre, *ACS Appl. Mater. Interfaces* **2018**, *10*, 5527–5533.
[27] S. J. Kang, H. Kim, S. Hwang, M. Jo, M. Jang, C. Park, S. T. Hong, H. Lee, *ACS Appl. Mater. Interfaces* **2018**, *11*, 517–524.
[28] N. N. Rajput, X. Qu, N. Sa, A. K. Burrell, K. A. Persson, *J. Am. Chem. Soc.* **2015**, *137*, 3411–3420.
[29] L. Lodovico, V. L. Martins, T. M. Benedetti, R. M. Torresi, *J. Braz. Chem. Soc.* **2014**, *25*, 460–468.
[30] Z. Ma, M. Kar, C. Xiao, M. Forsyth, D. R. MacFarlane, *Electrochem. Commun.* **2017**, *78*, 29–32.
[31] D. Aurbach, I. Weissman, Y. Gofer, E. Levi, *Chem. Rec.* **2003**, *3*, 61–73.
[32] N. Amir, Y. Vestfrid, O. Chusid, Y. Gofer, D. Aurbach, *J. Power Sources* **2007**, *174*, 1234–1240.
[33] J. Muldoon, C. B. Bucur, A. G. Oliver, T. Sugimoto, M. Matsui, H. S. Kim, G. D. Allred, J. Zajicek, Y. Kotani, *Energy Environ. Sci.* **2012**, *5*, 5941–5950.
[34] J. Muldoon, C. B. Bucur, T. Gregory, *Angew. Chem. Int. Ed.* **2017**, *56*, 12064–12084; *Angew. Chem.* **2017**, *129*, 12232–12253.
[35] R. Deivanayagam, B. J. Ingram, R. Shahbazian-Yassar, *Energy Storage Mater.* **2019**, *21*, 136–153.
[36] J. Zhang, X. Yao, R. K. Misra, Q. Cai, Y. Zhao, *J. Mater. Sci. Technol.* **2020**, *44*, 237–257.

[37] A. Lewandowski, A. Swiderska-Mocek, *J. Power Sources* **2009**, *194*, 601–609.
[38] G. A. Giffin, *J. Mater. Chem. A* **2016**, *4*, 13378–13389.
[39] G. T. Cheek, W. E. O'Grady, S. Z. El Abedin, E. M. Moustafa, F. Endres, *J. Electrochem. Soc.* **2008**, *155*, D91-D95.
[40] O. Shimamura, N. Yoshimoto, M. Matsumoto, M. Egashia, M. Morita, *J. Power Sources* **2011**, *196*, 1586–1588.
[41] D. Alwast, J. Schnaidt, K. Hancock, G. Yetis, R. J. Behm, *ChemElectroChem* **2019**, *6*, 3009–3019.
[42] F. Sagane, K. Ogi, A. Konno, K. Kanamura, *J. Electrochem. Soc.* **2019**, *166*, A5054-A5058.
[43] G. Vardar, A. E. S. Sleightholme, J. Naruse, H. Hiramatsu, D. J. Siegel, C. W. Monroe, *ACS Appl. Mater. Interfaces* **2014**, *6*, 18033–18039.
[44] S. Su, Y. NuLi, N. Wang, D. Yusipu, J. Yang, J. L. Wang, *J. Electrochem. Soc.* **2016**, *163*, D682-D688.
[45] H. Kuwata, M. Matsui, N. Imanishi, *J. Electrochem. Soc.* **2017**, *164*, A3229-A3236.
[46] J. Z. Hu, N. R. Jaegers, Y. Chen, K. S. Han, H. Wang, V. Murugesan, K. T. Mueller, *ACS Appl. Mater. Interfaces* **2019**, *11*, 38689–38696.
[47] T. Mandai, K. Tatesaka, K. Soh, H. Masu, A. Choudhary, Y. Tateyama, R. Ise, H. Imai, T. Takeguchi, K. Kanamura, *Phys. Chem. Chem. Phys.* **2019**, *21*, 12100–12111.
[48] T. J. Seguin, N. T. Hahn, K. R. Zavadil, K. A. Persson, *Front. Chem.* **2019**, *7*, 175–175(13).
[49] C. J. Pedersen, H. K. Frensdorff, *Angew. Chem. Int. Ed.* **1972**, *11*, 16–25; *Angew. Chem.* **1972**, *84*, 16–26.
[50] F. Tuerxun, Y. Abulizi, Y. NuLi, S. Su, J. Yang, J. Wang, *J. Power Sources* **2015**, *276*, 255–261.
[51] I. Shterenberg, M. Salama, H. D. Yoo, Y. Gofer, J. B. Park, Y. K. Sun, D. Aurbach, *J. Electrochem. Soc.* **2015**, *162*, A7118-A7128.
[52] P. Canepa, G. S. Gautam, R. Malik, S. Jayaraman, Z. Rong, K. R. Zavadil, K. Persson, G. Ceder, *Chem. Mater.* **2015**, *27*, 3317–3325.
[53] G. Giffin, A. Moretti, S. Jeong, S. Passerini, *J. Phys. Chem. C* **2014**, *118*, 9966–9973.
[54] T. Watkins, D. A. Buttry, *J. Phys. Chem. B* **2015**, *119*, 7003–7014.
[55] O. Tutusaus, R. Mohtadi, N. Singh, T. S. Arthur, F. Mizuno, *ACS Energy Lett.* **2017**, *2*, 224–229.
[56] Y. Shao, N. N. Rajput, J. Hu, M. Hu, T. Liu, Z. Wei, M. Gu, X. Deng, S. Xu, K. S. Han, J. Wang, Z. Nie, G. Li, K. R. Zavadil, J. Xiao, C. Wang, W. A. Henderson, J. G. Zhang, Y. Wang, K. T. Mueller, K. Persson, J. Liu, *Nano Energy* **2015**, *12*, 750–759.
[57] F. Sagane, K. Ogi, A. Konno, M. Egashira, K. Kanamura, *J. Electrochem. Soc.* **2016**, *84*, 76–78.
[58] A. Kitada, Y. Kang, Y. Uchimoto, K. Murase, *J. Electrochem. Soc.* **2014**, *161*, D102-D106.
[59] M. Matsui, *J. Power Sources* **2011**, *196*, 7048–7055.
[60] P. Jankowski, J. M. García Lastra, T. Vegge, *Batteries & Supercaps* **2020**, *3*, 1350–1359; Supercaps **2020**, 3, 1350–1359.
[61] D. Samuel, C. Steinhauser, J. G. Smith, A. Kaufman, M. D. Radin, J. Naruse, H. Hiramatsu, D. J. Siegel, *ACS Appl. Mater. Interfaces* **2017**, *9*, 43755–43766.
[62] J. D. Deetz, F. Cao, Q. Wang, H. Sun, *J. Electrochem. Soc.* **2018**, *165*, A61-A70.
[63] J. Z. Hu, N. N. Rajput, C. Wan, Y. Shao, X. Deng, N. R. Jaegers, M. Hu, Y. Chen, Y. Shin, J. Monk, Z. Chen, Z. Qin, K. T. Mueller, J. Liu, K. A. Persson, *Nano Energy* **2018**, *46*, 436–446.
[64] O. Borodin, W. Behl, T. R. Jow, *J. Phys. Chem. C* **2013**, *117*, 8661–8682.
[65] X. Qu, A. Jain, N. N. Rajput, L. Cheng, Y. Zhang, S. P. Ong, M. Brafman, E. Maginn, L. A. Curtiss, K. A. Persson, *Comput. Mater. Sci.* **2015**, *103*, 56–67.
[66] S. Kazemiabnavi, Z. Zhang, K. Thornton, S. Banerjee, *J. Phys. Chem. C* **2016**, *120*, 5691–5702.
[67] P. Peljo, H. H. Girault, *Energy Environ. Sci.* **2018**, *11*, 2306–2309.
[68] Y. Yu, A. Baskin, C. Valero-Vidal, N. T. Hahn, Q. Liu, K. R. Zavadil, B. W. Eichhorn, D. Prendergast, E. J. Crumlin, *Chem. Mater.* **2017**, *29*, 8504–8512.
[69] S. Plimpton, *J. Comput. Phys.* **1995**, *117*, 1–19.
[70] W. L. Jorgensen, D. S. Maxwell, J. Tirado-Rives, *J. Am. Chem. Soc.* **1996**, *118*, 11225–11236.
[71] J. N. Canongia Lopes, A. A. H. Pádua, *Theor. Chem. Acc.* **2012**, *131*, 1129.
[72] M. Brehm, B. Kirchner, *J. Chem. Inf. Model.* **2011**, *51*, 2007–2023.
[73] M. Brehm, M. Thomas, S. Gehrke, B. Kirchner, *J. Chem. Phys.* **2020**, *152*, 164105-164105–21.
[74] F. Neese, *WIREs Comput. Mol. Sci.* **2012**, *2*, 73–78.
[75] J. P. Perdew, *Phys. Rev. B* **1986**, *33*, 8822–8824.
[76] A. D. Becke, *Phys. Rev. A* **1988**, *38*, 3098–3100.
[77] F. Weigend, R. Ahlrichs, *Phys. Chem. Chem. Phys.* **2005**, *7*, 3297–3305.
[78] S. Grimme, J. Antony, S. Ehrlich, H. Krieg, *J. Chem. Phys.* **2010**, *132*, 154104.
[79] H. Kruse, S. Grimme, *J. Chem. Phys.* **2012**, *136*, 154101.
[80] V. Barone, M. Cossi, *J. Phys. Chem. A* **1998**, *102*, 1995–2001.
[81] M. M. Huang, Y. Jiang, P. Sasisanker, G. W. Driver, H. Weingärtner, *J. Chem. Eng. Data* **2011**, *56*, 1494–1499.
[82] A. B. Pereiro, H. I. M. Veiga, J. M. S. S. Esperança, A. Rodríguez, *J. Chem. Thermodyn.* **2009**, *41*, 1419–1423.

Manuscript received: November 22, 2020
Revised manuscript received: December 29, 2020
Accepted manuscript online: January 7, 2021